Dynamic Structures of Horse Liver Alcohol Dehydrogenase (HLADH): Results of Molecular Dynamics Simulations of HLADH-NAD^+-$PhCH_2OH$, HLADH-NAD^+-$PhCH_2O^-$, and HLADH-NADH-PhCHO

Jia Luo and Thomas C. Bruice*

Contribution from the Department of Chemistry and Biochemistry, University of California at Santa Barbara, Santa Barbara, California 93106

Received April 16, 2001

Abstract: Molecular dynamics simulations of the oxidation of benzyl alcohol by horse liver alcohol dehydrogenase (HLADH) have been carried out. The following three states have been studied: HLADH·$PhCH_2OH$·NAD^+ (MD1), HLADH·$PhCH_2O^-$·NAD^+ (MD2), and HLADH·PhCHO·NADH (MD3). MD1, MD2, and MD3 simulations were carried out on one of the subunits of the dimeric enzyme covered in a 32-Å-radius sphere of TIP3P water centered on the active site. The proton produced on ionization of the alcohol when HLADH·$PhCH_2OH$·NAD^+ → HLADH·$PhCH_2O^-$·NAD^+ is transferred from the active site to solvent water via a hydrogen bonding network consisting of serine48 hydroxyl, ribose 2′- and 3′-hydroxyl groups, and Hist51. Hydrogen bonding of the 3′OH of ribose to Ile269 carbonyl maintains this proton in position to be transferred to water. Molecular dynamic simulations have been employed to track water1287 from the TIP3 water pool to the active site, thus exhibiting the mode of entrance of water to the active site. With time the water1287 accumulates in two different positions in order to accept the proton from the ribose 3′-OH and from His51. There can be identified two structural substates for proton passage. In the first substate the imidazole Ne2 of His51 is adjacent to the nicotinamide ribose C2′-OH and hydrogen bonding distances for proton transfer through the hydrogen bonded relay series $PhCH_2OH$···Ser48-OH···Ribose2′-OH···His51···OH_2 (path **1**) average 2.0, 2.0, and 2.1 Å and (for His51···OH_2) minimal distances less or equal to 2.5 Å. The structure for path **1** is present 20% of the time span. And in the second substate, there are two possible proton passages: path **1** as before and path **2.** Path **2** involves the hydrogen-bonded relay series $PhCH_2OH$···Ser48-OH···Ribose2′-OH···Ribose3′-OH···His51···OH_2 with the average bonding distances being 2.0, 2.0, 2.1, and 2.0 Å and (for His51····OH_2) minimal distances less or equal to 2.5 Å (20% probability of the time span), respectively. During the molecular dynamics simulation the NAD^+ ribose conformations have stabilized at the C2′-*endo*−C3′-*exo* or the C2′-*endo* conformations. With the C2′-*endo* conformation the first and second substates are able to persist for different time spans, while with the C2′-*endo*−C3′-*exo* conformation the only possible pathway involves the first substate. For both first and second substates the fluctuation of the distances between the ribose-OH protons and Nϵ2 of His51 imidazole ring is partially contributed by the "windshield wiper" motion of the His51 imidazole ring. Since the imidazole of His-51 contributes only about 10-fold to activity, as estimated from the decrease in activity upon substitution with a Gln, there must be an alternate route for the proton to pass to solvent without going through this histidine. A third pathway involves ribose C3′-OH and Ile-269. In MD2, near attack conformers (NACs) for hydride transfer from $PhCH_2O^-$ to NAD^+ represent ∼60% of E·S conformers. The molecular dynamic study of MD3 at mildly basic pH reveals that reactive ground state conformers (NACs) for hydride transfer from NADH to PhCHO amount to 12 mol % of conformers. In MD3, anisotropic bending of the dihydronicotinamide ring of NADH (average value of $\alpha_c = 4.0°$ and $\alpha_n = 0.5°$, respectively) is observed.

Introduction

Horse liver alcohol dehydrogenase (HLADH, EC 1.1.1.1)[1] has a molecular weight of 80 000 and is a dimer of two identical subunits as reported in the X-ray structure.[2] The enzyme has a twelve-stranded β-pleated sheet, which makes up the central core of the dimer. Each subunit of this dimeric enzyme binds one molecule of NAD^+ and two Zn(II) ions. One zinc is in the active site, while the other is structural. Upon enzyme substrate complex formation a rigid body rotation closes the cleft between the coenzyme and catalytic domains. This conformational change is described by a rotation of 9° to 10° in the monoclinic form. The hydroxyl oxygen of the alcohol substrate is ligated to the active site zinc. The oxidation involves alcohol hydroxyl proton ionization and passage of the H^+ through a hydrogen bond network to water via His51 imidazole and hydride transfer from alkoxide to NAD^+ (eq 1).

$$\{\text{E-NAD}^+\text{-RCH}_2\text{OH}\} \rightleftharpoons \{\text{E-NAD}^+\text{-RCH}_2\text{O}^-\} + \text{H}^+ \quad (1)$$

$$\{\text{E-NAD}^+\text{-RCH}_2\text{O}^-\} \rightleftharpoons \{\text{E-NADH}-\text{RCHO}\}$$

Molecular dynamics simulations on HLADH·NAD^+ systems with varied substrates have been reported.[3−8] Ryde[3] used a

10.1021/ja0109747 CCC: $20.00
Published on Web 11/08/2001

HLADH·NADH system to test the calculated force field and geometry for the active site zinc related terms in a 40 ps molecular dynamics run. The test was focused on the coordination sphere of zinc when it is bound to water and His as well as Cys ligands. The simulation was performed for one of the active sites and with the area close to the active site included. The studies by Olson[4] and Vanhomnerig[5] and their co-workers were to 100 ps with one of the two subunits fixed during the MD simulations. Pavelites et al.[6] used a HLADH·NAD^+·ethanol MD simulation to test their force field for nicotinamide adenine dinucleotides. Alhambra et al.[7] more recently used a QM/MM approach to calculate and compare the kinetic isotope effects for oxidation of alcohols by this enzyme. Agarwal et al.[8] reported a 100 ps molecular dynamics study of this system with the substrate being benzyl alcohol and benzyl alkoxide, using the GROMOS force field.

In this article we report molecular dynamics (MD) simulations carried into the nanosecond time range on HLADH·NAD^+·$PhCH_2OH$ (the reactant state, MD1), HLADH·NAD^+·$PhCH_2O^-$ (the intermediate state, MD2), and HLADH·NADH·PhCHO (the product state, MD3) complexes. Molecular dynamics simulations allowed us to probe the dynamics of the proton relay, the stabilization of intermediate $PhCH_2O^-$, and the near attack conformations (NACs) through which the transition state for hydride transfer is reached.[9]

Methods

Starting structures with HLADH for molecular dynamics investigations, using the program CHARMM[10] (Version 25b2), were obtained by a best-fit superimposition of benzyl alcohol/benzyl alkoxide/benzaldehyde on the pentafluorobenzyl alcohol, bound to the active site Zn(II) ion in both of the dimeric subunits of the X-ray structure at 2.1 Å resolution.[2] The resulting configurations were then used for molecular dynamics with systems MD1, MD2, and MD3 (vide infra). CHARMM was used to add all hydrogens in the crystal structure, including the crystallographic waters. The dynamics are treated by stochastic boundary conditions.[11−13] The crystal structure was placed into a 32 Å in radius sphere of TIP3P water[14] centered on the midpoint of a line from the donor carbon of $PhCH_2OH$ to the C4 of the nicotinamide in the active site (Figure 1). A shell from 30 to 32 Å forms the buffer zone and is treated with constrained Langevin dynamics[11−13] with a stochastic heat bath at 300 K by randomly fluctuating and dissipative forces. A frictional coefficient of 62 ps^{-1} was placed on the oxygen atom of any water molecule more than 30 Å from the center of the sphere. Any water molecule within 2.6 Å of the enzyme complex or a crystallographic water was deleted. The system consisted of a total of 18 022 atoms. The CHARMM residue topology file was used for the enzyme residues[10] and zinc. NAD^+ and NADH developed by Pavelites and co-workers[3] were used. The partial charges and parameters for substrates were treated as in our earlier studies.[4,15,16] The Dynamics to 1.5 (MD1 and MD3) and 2 ns (MD2) were run with use of Verlet integration at a time step of 0.001 ps (1000 steps/ps). Bonds containing hydrogens were constrained by using the SHAKE algorithm[17] during molecular dynamics. The following protocol was used: The assembly was minimized prior to dynamics studies, and 100 steps of the steepest descent algorithm minimization with a force criterion of 0.001 kcal/10 steps were followed by the adopted basis Newton−Raphson algorithm for 2000 steps (tolerance 1×10^{-9} kcal/10 steps). Nonbonded interactions were cut off at 14.0 Å, and were updated every 25 steps. The system was heated to 300 K, followed by initial equilibration of 80 and 1420 ps of observation for MD1 and MD3 and 1920 ps for MD2. Coordinates were saved every 0.1 ps, giving 14 200 structures, and the final 8000 collection phase structures were used for analyses. Calculations were carried out on SGI indigo workstations. Structural visualization and manipulation of these structures was performed by using MidasPlus (UCSF) and Quanta, version 4.0 (MSI, currently Biosym/MSI, San Diego, CA).

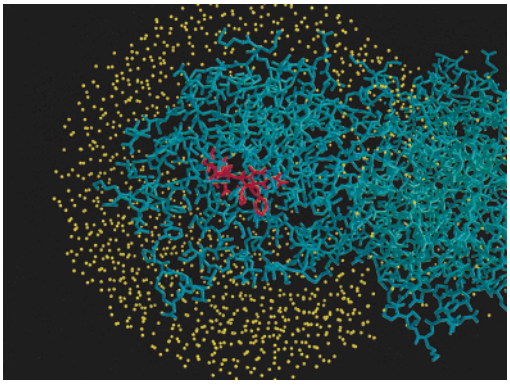

Figure 1. One subunit of the crystal structure of the dimeric HLADH enzyme (cyan) that has been placed into a 32 Å in radius sphere of TIP3P water (yellow). The water sphere is centered on the midpoint of a line from the donor carbon of $PhCH_2OH$ (red) to the C4 of the nicotinamide (red) in the active site.

Results and Discussions

Molecular dynamics simulations were performed on the following assemblies of the dimeric alcohol dehydrogenase: (MD1) enzyme with NAD^+ and $PhCH_2OH$ at the active site; (MD2) enzyme with NAD^+ and $PhCH_2O^-$ at the active site; and (MD3) enzyme with NADH and PhCHO at the active site. Preparation of the constructs (MD1 to MD3) is described in the Methods section. The molecular dynamics results and statistical analyses are from the final 800 ps of molecular dynamics simulations. Detailed results of these simulations are presented in the following sections.

Proton Shuttling from the Active Site of HLADH·NAD^+·$PhCH_2OH$ Complex (MD1). The hydroxyl oxygen of $PhCH_2$-OH remains associated with the active site zinc during the dynamics run. The complexation of benzyl alcohol by Zn^{2+} lowers the pK_a of the alcohol hydroxyl group. The first step of

(1) Brändén, C. I.; Jörnvall, H.; Eklund, H.; Furugren, B. *The Enzymes*, 3rd ed.; Boyer, P. D., Ed.; Academic Press: New York, NY, 1975; Vol. 11, p 103.
(2) Ramaswamy, S.; Eklund, H.; Plapp, B. V. *Biochemistry* **1994**, *33*, 5230−5237.
(3) Ryde, U. *Int. J. Quantum Chem.* **1994**, *52*, 1229−1243. Ryde, U. *Protein Struct. Funct. Genet.* **1995**, *21*, 40−56.
(4) Olson, L. P.; Luo, J.; Bruice, T. C. *Biochemistry* **1996**, *35*, 9782−9791.
(5) Vanhommerig, S. A. M.; Sluyterman, L. A. Æ.; Meijer, E. M. *Biochim. Biophys. Acta* **1996**, *1295*, 125−138.
(6) Pavelites, J. J.; Gao, J.; Bash, P. A.; Mackerell, A. D., Jr. *J. Comput. Chem.* **1997**, *18*, 221−239.
(7) (a) Alhambra, C.; Corchado, J. C.; Luz Sanchez, M.; Gao, J.; Truhlar, D. G. *J. Am. Chem. Soc.* **2000**, *122*, 8197. (b) Private communication from these authors.
(8) Agarwal, P. K.; Webb, S. P.; Hammes-Schiffer, S. *J. Am. Chem. Soc.* **2000**, *122*, 4803−4812.
(9) Bruice. T. C.; Lightstone, F. C. *Acc. Chem. Res.* **1999**, *32*, 127−136.
(10) Brooks, B. R.; Bruccoleri, R. E.; Olafson, B. D.; States, D. J.; Swaminathan, S.; Karplus, M. *J. Comput. Chem.* **1983**, *4*, 187−217.
(11) Brooks, C. L.; Brunger, A.; Karplus, M. *Biopolymers* **1985**, *24*, 843.
(12) Brooks, C. L.; Pettitt, B. M.; Karplus, M. *J. Chem. Phys.* **1985**, *83*, 5897.
(13) Chandresekhar, S. *Rev. Mod. Phys.* **1943**, *15*, 1.
(14) Jorgensen, W. L.; Chandrasekhar, J.; Madura, J. D. *J. Chem. Phys.* **1983**, *79*, 926−935.
(15) Almarsson, Ö.; Karaman, R.; Bruice, T. C. *J. Am. Chem. Soc.* **1992** *114*, 8702; Almarsson, Ö.; Bruice, T. C. *J. Am. Chem. Soc.* **1993**, *115*, 2125−2138. Almarsson, Ö.; Sinha, A.; Gopinath, E.; Bruice, T. C. *J. Am. Chem. Soc.* **1993**, *115*, 7093−7102.
(16) Luo, J.; Kahn, K.; Bruice, T. C. *Bioorg. Chem.* **1999**, *27* (4), 289−296.
(17) van Gunsteren, W. F.; Berendsen, H. J. C. *Mol. Phys.* **1977**, *34*, 1311.

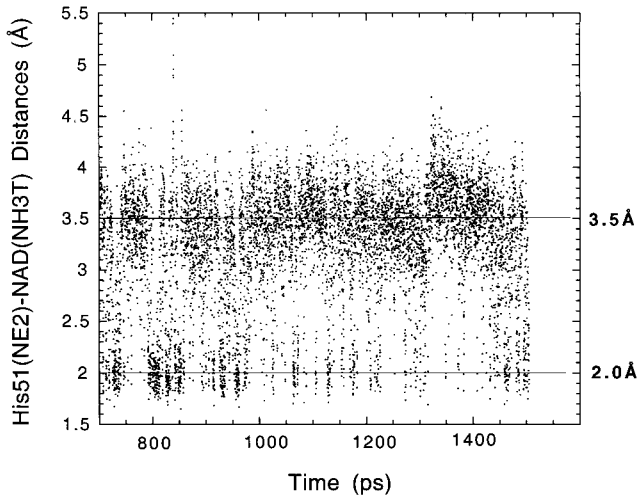

Figure 2. Hydrogen bonding histograms of the time-dependent distances between the ribose 3′ hydroxyl proton, NH3T, and the Nϵ2 of His51. The two average distances 2.0 ± 0.3 (range 1.7−2.4 Å) and 3.5 ± 0.7 Å (range 2.8−4.2 Å) pertain to substates 1 and 2, respectively. The first substate appears ∼80% of the time and the second substate about ∼20% of the time.

Table 1. Heavy Atom Distances at the Active Site for MD1

atoms		distances (Å)
NC4	C7	3.73
O1	48OG	2.65
48OG	NO2′	2.85
NO2′	51NE2	3.39
NO2′	NO3′	2.89
NO3′	51NE2	3.66[a]
NO3′	269O	2.71
51ND1	WatAO	3.30
51NE2	WatAO	2.99
269O	WatBO	2.90
Zn	O1	2.63

[a] C2′-*endo* conformation. For the C2′-*endo*−C3′-*exo* conformation this distance is >4.5 Å.

the oxidation of $PhCH_2OH$ by NAD^+ involves H^+ dissociation. It has been proposed[18] that the dissociated H^+ is shuttled from the active site to solvent water by a series of −O−H···O− hydrogen bonds. We find two substates in this simulation in Chart 1. The main difference in these two substates is the distances between the hydrogen of ribose C3′-OH and His51 Ne2. The ribose C3′ hydroxyl proton is found at one of two average distances to the His51 Nϵ2 referred to as substate 1 and substate 2 (Figure 2). The proton relay in both substates consists of a hydrogen bond between $PhCH_2OH$ and Ser48 hydroxyl oxygen (Chart 1). The Ser48-OH is hydrogen bonded to the oxygen of ribose C2′-OH which is, in turn, bifurcated hydrogen bonded to His51 Nϵ2 and to the ribose C3′-OH. In addition, the ribose C3′-OH forms a hydrogen bond with the carbonyl oxygen of Ile-269 in both substates. However, the ribose C3′-OH also forms a bifurcated hydrogen bond with His51 Nϵ2 in substate 2; this hydrogen bond is mostly beyond 3 Å in substate 1. Substate 2 is found ∼20% of the time during MD1. With the exception of the ribose C2′-*endo* and C2′-*endo*−C3′-*exo* conformations, the heavy atom positions in substates 1 and 2 are identical (Table 1) and the placement of functional groups is shown in Figure 3. From the MD1 simulation the hydrogen bond distances of the benzyl alcohol hydroxyl proton from the Ser48 hydroxyl oxygen are 2.0 ± 0.2 Å (range 1.8−2.5 Å). The average distance of the Ser48 hydroxyl proton from the NAD^+ ribose 2′-OH oxygen is 2.0 ± 0.2 Å (range 1.8−2.2 Å). The ribose C2′-hydroxyl proton is at an average hydrogen bonding distance to the C3′-hydroxyl oxygen of 2.1 ± 0.2 Å (range 1.9−2.3 Å), and to the His51 Nϵ2 of 2.1 ± 0.3 Å (range 1.8−2.6 Å). The ribose 3′ hydroxyl proton is found at one of two average distances to the His51 Nϵ2, in substate 1 the distance is 2.0 ± 0.3 Å (range 1.7−2.4 Å) and in substate 2 the distance is 3.5 ± 0.7 Å (range 2.8−4.2 Å) (Figure 2).

In substate 1, when the imidazole Nϵ2 is adjacent to C2′-OH, the hydrogen bonding distances are in accord with a plausible concerted proton transfer through the hydrogen bonded relay series $PhCH_2OH$···Ser48-OH···Ribose2′-OH···His51···OH_2 (path 1, labeled as **1** in Chart 1) with average bonding distances 2.0, 2.0, and 2.1 , and (for His51····OH_2) minimal distances less or equal than 2.5 Å (15% probability of time span), respectively, as shown in Chart 1. In the second substate, there are two possible proton passages: path **1** as above and path 2 (labeled as **2** in Chart 1). Path **2** involves the hydrogen bonded relay series $PhCH_2OH$···Ser48-OH···Ribose2′-OH···Ribose3′-OH···His51···OH_2 with the average bonding distances being 2.0, 2.0, 2.1, and 2.0 Å and (for His51···OH_2) minimal distances less than or equal to 2.5 Å (15% probability of time span), respectively, as shown in Chart 1. At ∼500 ps the nicotinamide ribose conformation has converged to C2′-*endo*−C3′-*exo* and C2′-endo conformations; with the C2′-*endo* conformation the first and second substates are able to reside at different time spans, while with the C2′-*endo*−C3′-*exo* conformation the only possible pathway involves the first substate. For both first and second substates the fluctuation of the distances between the ribose-OH protons and ϵN of the His51 imidazole ring are partially contributed by the "windshield wiper" motion of the His51 imidazole ring. However, in both substates the proton can also be passed to a nearby water (labeled as **3** in Chart 1) through the ribose C3′-OH hydrogen bonded to the carbonyl oxygen of Ile-269 and then to the water channel leading to the surface of the protein. The ribose 3′-OH proton is hydrogen bonded to the carbonyl oxygen of Ile-269 (1.8 ± 0.1 Å, range 1.7−2.4 Å) and the carbonyl oxygen is hydrogen bonded to a nearby water molecule (2.0 ± 0.2 Å, range 1.8−2.2 Å).

Based on X-ray data, the transfer of the H^+ from nicotinamide ribose (3′ hydroxyl proton and 2′ hydroxyl proton) has been proposed[2] to be to the Nϵ2 of the imidazole ring of His51. Subsequently, transfer of the H^+ from the generated His51-ImH^+ (proton on Nϵ2) to water was proposed to take place at either the Nδ1 or Nϵ2 of His51. In the molecular dynamics simulation both structurally allowed pathways (Nδ1 and Nϵ2) to water are observed (compare Chart 1 and Figure 3). The transfer of the proton through the C3′-OH and C2′-OH function to the Nϵ2 of His51 (Chart 2, intermediate state) [and then to Water-860 (2.5 Å) and subsequently to a hydrogen bonded (2.2 Å) nearby water] is intermittent due to the dynamic motion of the imidazole of His51. An X-ray structure at 1.25 Å resolution (unpublished results)[19] of a benzyl alcohol complex with HLADH·NAD^+ has been reported to have the alcohol/alkoxide O and O of Ser48 at a distance of 2.5 Å. Based on this O−O distance and the observation of an inverse k^D/k^H isotope effect, a low barrier hydrogen bond was proposed for the $PhCH_2O^-$···H-hydrogen bond in Chart 2.

Since the imidazole of His51 contributes only about 10-fold to activity, as estimated from the decrease in activity upon

(18) Eklund, H.; Plapp, B. V.; Samama, J.-P.; Brändén, C.-I. *J. Biol. Chem.* **1982**, *23*, 14349−14358.

(19) Ramaswamy, S.; Park, D. H.; Plapp, B. V. *Biochemistry* **1999**, *38*, 13951−13959.

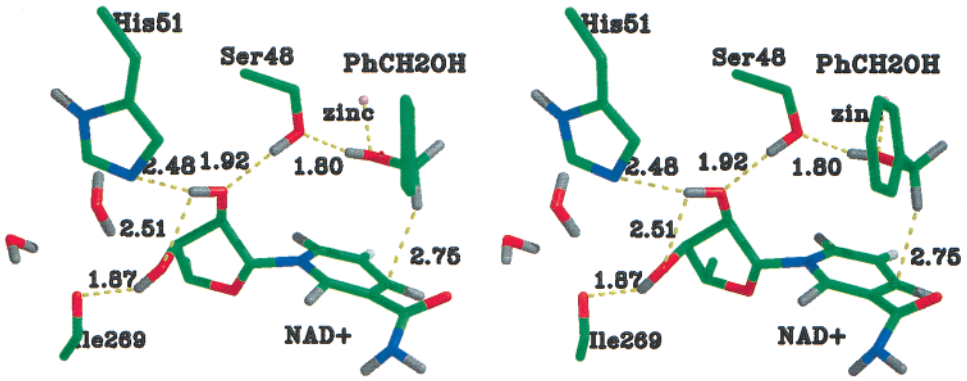

Figure 3. Stereosnapshot of the three-dimensional structure of the active site portion in MD1. The *pro*-R hydrogen of benzyl alcohol poised to transfer to C4 of NAD^+ and the hydrogen bonding network consists of the Ser48 proton hydrogen bonded to the oxygen of ribose C2′-OH, which is hydrogen bonded to both Nϵ2 of His51 and the ribose C3′-OH which forms a hydrogen bond with the carbonyl oxygen of residue 269. The distance between the ribose C3′-OH proton and the Water1287 oxygen is 3.60 Å. The distances between the His51 Nϵ2 and Nδ1 and the oxygen of Water860 are 2.99 and 3.30 Å, respectively.

Chart 1

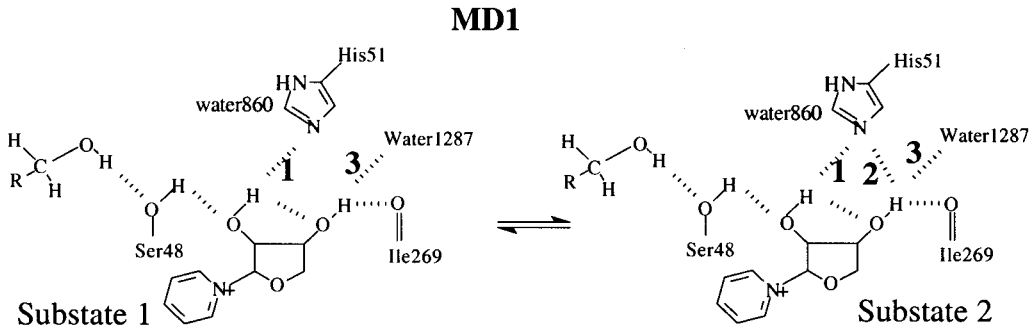

Chart 2

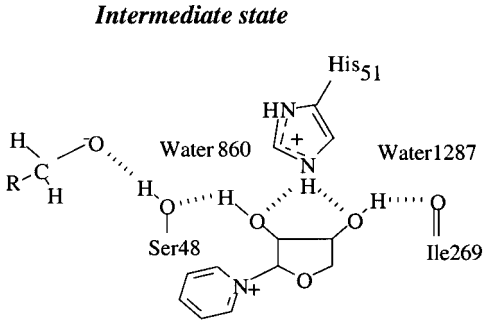

substitution with a Gln,[20] there must be an alternate route for the proton to pass to solvent without going through this histidine. This is consistent with transfer of H^+ involving hydrogen bond **3** as shown in Chart 1 where the Nicotinamide ribose 3′-OH is hydrogen bonded to the carbonyl oxygen of Ile-269 (1.8 Å). Hydrogen bonding of the 3′-OH of ribose to Ile269 carbonyl maintains this proton in position to be transferred to water. The nicotinamide ribose C3′-OH proton is at a minimal distance of 3.1 Å to the oxygen of water1287. This path of proton transfer comprises an alternate path for the H^+ to reach the surface of the enzyme.

The Structure in the Active Site of HLADH·NAD^+·$PhCH_2O^-$ Complex (MD2) after 2 ns Simulation. What follows deals with the structure of HLADH·NAD^+·$PhCH_2O^-$ complex after acid dissociation of $PhCH_2OH$ and the transfer of the proton to water (Chart 3). The heavy atom distance in MD2 is provided in Table 2. The alkoxide oxygen of $PhCH_2O^-$ is stabilized by association with the active site zinc. Several MD simulations were initiated with the Ser48-OH hydrogen bonded to the $PhCH_2O^-$ oxygen. In each study the proton of Ser48-OH flipped away from the alkoxide oxygen to hydrogen bond to the ribose C2′OH at about 50 ps. From the histograms the alkoxide O and the OG of Ser48 are separated by only 2.92 ± 0.20 Å (range 2.60−3.20 Å); however, the Ser48-OH proton does no reside between these oxygens. When placed between the alkoxide and Ser48 oxygens the proton moved away to the positioning shown in Figure 5.

The average distance of the alkoxide oxygen and the Ser48-OH proton is 2.90 ± 0.30 Å (range 2.50−3.40 Å) (see Figure 4). The average distance of the Ser48-OH proton from the ribose C2′-OH O is 1.80 ± 0.15 Å (range 1.65−2.00 Å) (Figure 4b). The ribose C2′-hydroxyl proton is at an average hydrogen bonding to the NAD^+ C3′-hydroxyl oxygen of 2.1 ± 0.2 Å (range 1.9−2.3 Å) and an average hydrogen bonding to the His51 at the Nϵ2 position of 2.6 ± 0.6 Å (range 2.0−3.4 Å). With time the ribose C3′ hydroxyl proton resides at one of two average distances to the Nϵ2 position of His51. These distances are 2.0 ± 0.2 (range 1.8−2.3 Å) and 3.5 ± 0.5 Å (range 3.0−4.0 Å), respectively.

Hydride Transfer in the (MD2) HLADH·NAD^+·$PhCH_2O^-$ Complex. Figure 5 shows the *pro*-R hydrogen of $PhCH_2O^-$ pointing almost directly at C4 of the NAD^+. In Figure 6 there is presented a plot of the distance between the *pro*-R hydrogen H1 of $PhCH_2O^-$ and C4 of the nicotinamide ring of NAD^+ (average H_R to C4 distance, 2.7 Å) vs the $PhCH_2O^-$ to nicotinamide virtual angle C7−H1···C4. Included in Figure 6 are 8000 conformations from the MD2 simulations. Examination of Figure 6 shows the proximity of transferring *pro*-R hydrogen H1 of $PhCH_2O^-$ and C4 of NAD^+ to be as close as 2.3 Å. The

(20) Ehrig, T.; Hurley, T. D.; Edenberg, H. G.; Bosron, W. F. *Biochemistry* **1991**, *30*, 1062−1068.

Chart 3

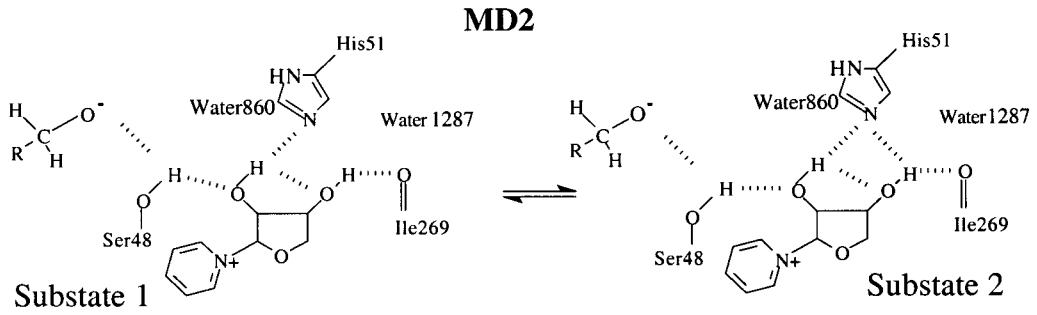

Table 2. Heavy Atom Distances at the Active Site for MD2

atoms		distances (Å)
NC4	C7	3.79
O1	48OG	2.81
48OG	NO2′	2.70
NO2′	51NE2	3.16
NO2′	NO3′	2.81
NO3′	51NE2	3.11
NO3′	269O	2.68
51ND1	WatAO	3.35
51NE2	WatAO	3.62
269O	WatBO	2.53
Zn	O1	1.96

near attack conformations (NACs) are included in the box at the lower right-hand corner of Figure 6. The NAC structures, which are present as ∼60% of conformers, are those with hydride transfer distances (H_R to C4) and angles (C7−H1···C4) of ≤3.0 Å and ≥132°.[21]

From X-ray data it has been proposed that the proton generated by acid dissociation of $PhCH_2OH$ is eventually passed to His51 Nϵ2 and transferred to a nearby water via Nδ1 and to the surface water by way of a water channel. Due to the ready migration of water molecules, their positions and migratory paths are best understood via MD simulations. In Figure 7 we show the pathway for the bulk water1287 from the TRIP3 water pool to the vicinity of NAD^+ ribose, His51 and Ile269. In Figure 8 we see the positions that water1287 takes during a 1 nsc time period. Note that water1287 is in position to accept the H^+ from Nδ1 of His 51 and the ribose 3′-OH, which is associated with Ile269.

The Reversibility of MD2 → MD3 at Neutral and Basic pH. Molecular dynamic simulation of the HLADH·NADH·PhCHO species was carried out. From a plot of the distances from the *pro*-R hydrogen of NADH to the carbonyl carbon of PhCHO vs the angle formed by C4 to the *pro*-R hydrogen to C7 of PhCHO no formation of NAC species was found. From this result the reaction would be highly unfavorable. Examination of the structure revealed that when compared to the structure of MD2, the benzene ring of the aldehyde had shifted positions while the distance of the aldehyde carbonyl oxygen and the Zn^{2+} had remained constant. Such alternative positions are observed in the X-ray structures of various HLADH complexes.[22] The Ph- moiety of PhCHO was repositioned to the original position in the X-ray structure and the system subjected to 200 ps MD simulation. In the alternate conformation, so obtained, the distances between the *pro*-R hydrogen of NADH and C7 of aldehyde were as before but the angles formed by C4 of NADH to the *pro*-R hydrogen to the C7 of aldehyde were found to sample more of the NAC conformation employing the same definition of NAC structures used for the MD2 study. Heavy atom distances for this MD3 structure are provided in Table 3 and a stereoview of the structure in Figure 9. It was found from a plot of the distances from the *pro*-R hydrogen of NADH to the carbonyl carbon of PhCHO vs the angle formed by C4 to the *pro*-R hydrogen to C7 of PhCHO that ∼12 mol % of NAC conformers are present with time (Figure 10).

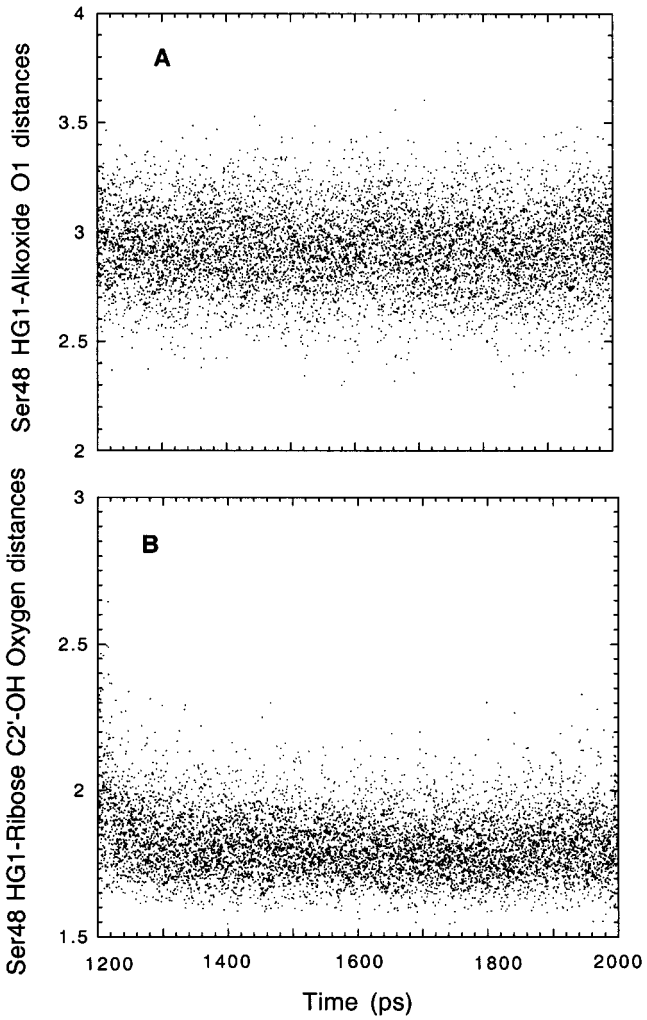

Figure 4. Histograms for MD2: (A) distance between the Ser48 hydroxyl proton and alkoxide O; (B) distance between the ribose C2′-OH oxygen and the Ser48 hydroxyl proton.

(21) The definition of a NAC for hydride transfer to NAD^+ of ≤3.0 Å H1 to C4 distance and C7−H1···C4 angle of ≥132° was previously used in the MD simulation of reduction of NAD^+ by formate in a study of formate dehydrogenase.[26] The C7−H1···C4 angle in the transition states for over the barrier H^- transfer is 155−163° while for H^- transfer by tunneling it is 152° (ref 7b). The angles for the NACs were defined to be from 132° to 180°. The use of a single, though arbitrary, definition of a NAC allows comparisons between different NAD^+/NADH enzymes.

(22) Ramaswamy, S.; Scholze, M.; Plapp, B. V. *Biochemistry* **1997**, *36*, 3522−3527.

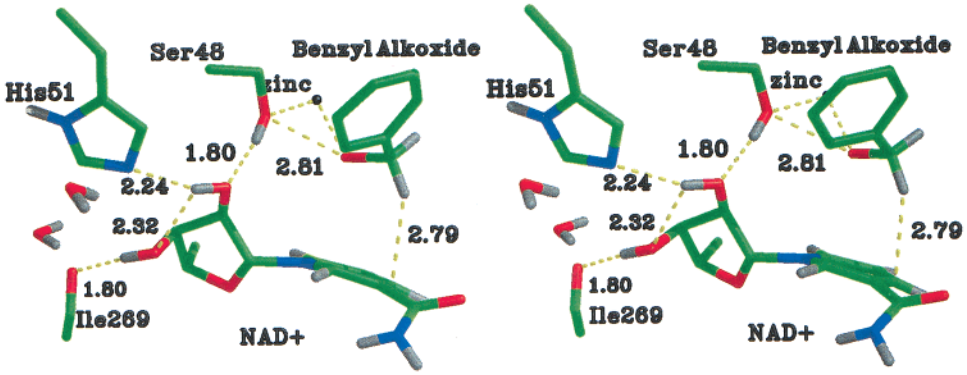

Figure 5. Stereosnapshot of the three-dimensional structure of the active site portion in MD2. The *pro*-R hydrogen of benzyl alkoxide poised to transfer to C4 of NAD^+ and the hydrogen bonding network consisting of the Ser48 proton hydrogen bonded to the oxygen of ribose C2′-OH which is hydrogen bonded to both Nϵ2 of His51 and the ribose C3′-OH which, in turn, forms a hydrogen bond with carbonyl oxygen of residue 269. The distance between the ribose C3′-OH proton and the Water1287 oxygen is 3.70 Å. The distances between the His51 Nϵ2 and Nδ1 and the oxygen of Water860 are 3.62 and 3.35 Å, respectively.

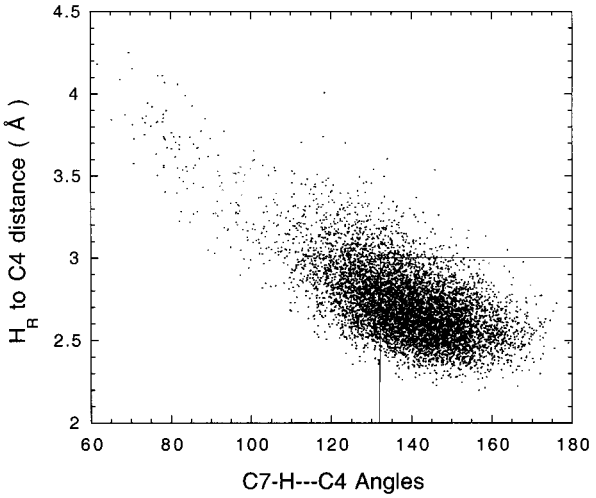

Figure 6. The distance between the *pro-R* hydrogen H1 of $PhCH_2O^-$ and C4 of the nicotinamide ring of NAD^+ (average H_R to C4 distance, 2.7 Å) vs the $PhCH_2O^-$ to nicotinamide virtual angle C7−H1···C4. Included in Figure 6 are 8000 conformations from the MD2 simulations. The near attack conformations (NACs) are included in the box at the lower right-hand corner. The NAC structures, which are present as ~60% of conformers, are those with hydride transfer distances (H_R to C4) and angles (C7−H1···C4) of ≤3.0 Å and ≥132°.[21]

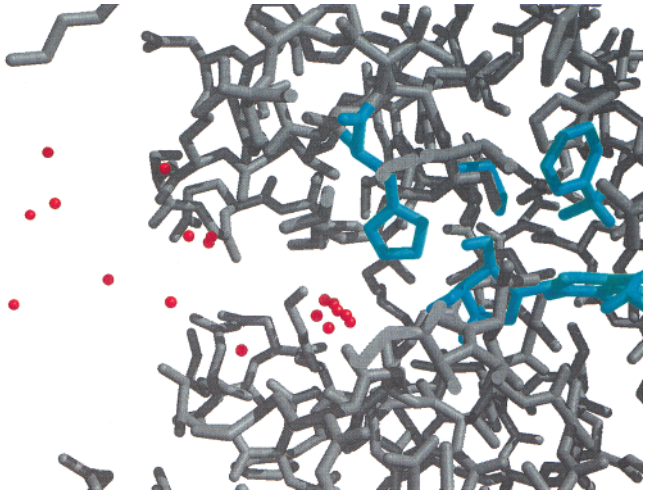

Figure 7. The pathway for the bulk water1287 (red balls) from the TRIP3 water pool to the vicinity of of the enzyme (gray) housing the ribose of NAD^+, His51, and Ile269 (cyan).

Acid Catalysis of the Reduction of Aldehyde by NADH. The conditions for the oxidation of $PhCH_2O^- \rightarrow PhCHO$ by HLADH·NAD^+ include a basic pH. The reduction of $PhCHO \rightarrow PhCH_2OH$ by HLADH·NADH requires an acidic pH.[23] The structure of the ground state E·S complex at acid pH must differ from that at basic pH. Presumably at acidic pH His51-Im is protonated and proton transfer from His51-ImH^+ is either concerted with hydride transfer or traps the $PhCH_2O^-$ moiety. We have yet to perform molecular dynamics on the HLADH·NADH·$PhCH_2O^-$ species with a protonated His51.

There has been some discussion about the presence and importance of the ring puckering of 1,4-dihydropyridine (Chart 4) on hydride transfer from NADH.[15,24,25] We have examined several dehydrogenase enzymes[15,16] with substrate and NAD(P)H or NADH cofactors at the active site using molecular dynamics simulations and shown that, most usually, a bulky amino acid residue on the face of the dihydropyridine ring distal to the substrate induces anisotropic bending of the nicotinamide ring, toward the substrate. (A notable exception is formate dehydrogenase.[26]) In the instance of HLADH the bulky residue is Val 203.[16] This steric protection of the space on the unreactive face of NADH and the resultant anisotropic bending of the NADH in the direction of the substrate is responsible for the stereospecificity of a number of dehydrogenase enzymes (A side vs B side) and the energetics of the hydride transfer step. The puckering of the 1,4-dihydronicotinamide ring places one of the C4-hydrogens of NADH in a *pseudo*axial position and the other C4-hydrogen in the *pseudo*equatorial position. Hydride transfer involves the pseudoaxial hydrogen for which the bond energy has been calculated to be ca. 80 kcal/mol compared to a bond energy of ca. 109 kcal/mol for the pseudoequatorial hydrogen.[27] That the ring puckering and pyramidalization at the ring nitrogen does have a significant energetic consequence according to the calculations may be attributed to the increase in driving force for hydride expulsion due to an increased

(23) Kvassman, J.; Pettersson, G. *Eur. J. Biochem.* **1980**, *103*, 557−564. Kvassman, J.; Pettersson, G. *Eur. J. Biochem.* **1980**, *103*, 565−575. Klinman, J. P., et al. *J. Biol. Chem.* **1975**, *250*, 2569.

(24) Rotberg, N. S.; Cleland, W. W. *Biochemistry* **1991**, *30*, 4068.

(25) Wu, Y.-D.; Houk, K. N. *J. Am. Chem. Soc.* **1987** *109*, 906. Wu, Y.-D.; Houk, K. N. *J. Am. Chem. Soc.* **1987** *109*, 2226. Wu, Y.-D.; Houk, K. N. *J. Am. Chem. Soc.* **1991**, *113*, 2353−2358. Wu, Y.-D.; Houk, K. N. *J. Org. Chem.* **1993**, *58*, 2043−2045. Wu, Y.-D.; Lai, D. K. W.; Houk, K. N. *J. Am. Chem. Soc.* **1995**, *117*, 4100−4108.

(26) Torres, R.; Schiøtt, B.; Bruice, T. C. *J. Am. Chem. Soc.* **1999**, *121*, 8164−8173.

(27) Oppenheimer, N. J.; Arnold, L. J., Jr.; Kaplan, N. O. *Biochemistry* **1978**, *17*, 2613.

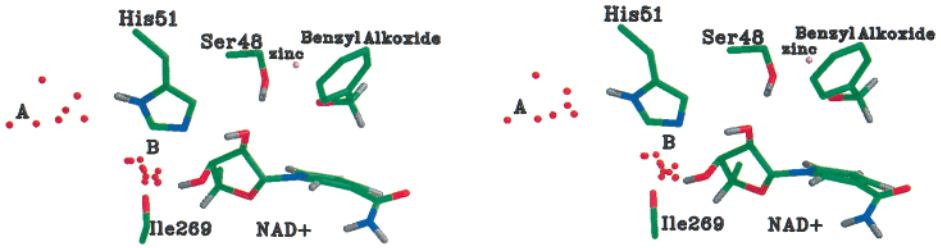

Figure 8. A stereoview of the active site of MD2, which exhibits the positions of residence of water1287 during a 1 nsc time period. Note that water1287 is in position to accept the H^+ from Nδ1 of His 51 and the ribose 3′-OH that is associated with Ile269.

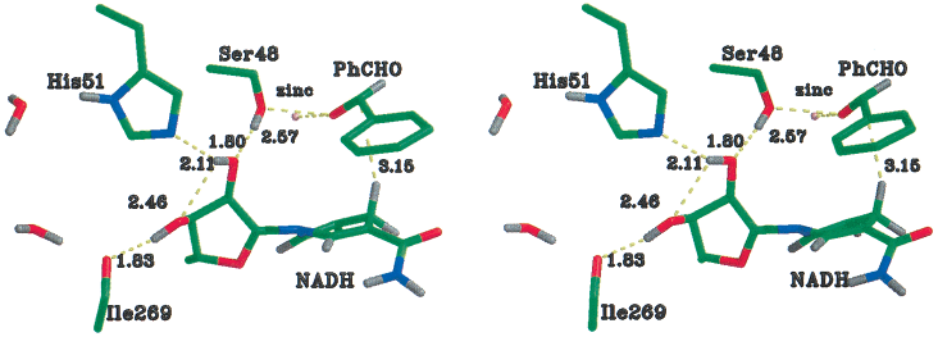

Figure 9. Stereosnapshot of the three-dimensional structure of the active site portion in MD3. The *pro*-R hydrogen of NADH poised to transfer to C7 of benzyl aldehyde and the hydrogen bonding network consists of the Ser48 proton hydrogen bonded to the oxygen of ribose C2′-OH that is hydrogen bonded to both Ne2 of His51 and the ribose C3′-OH which forms a hydrogen bond with the carbonyl oxygen of residue 269.

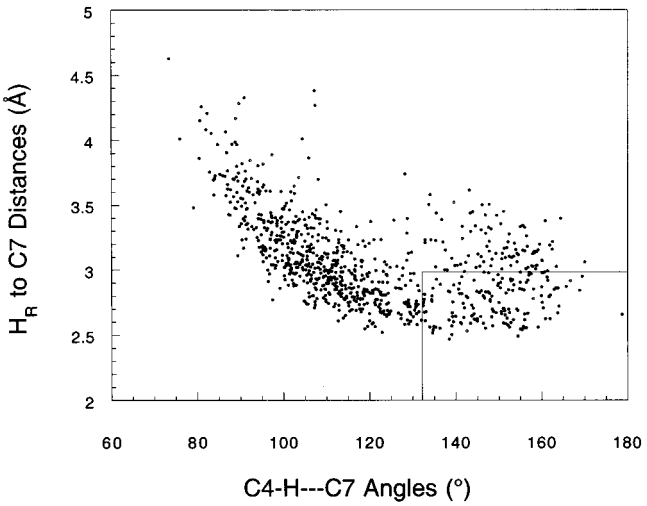

Figure 10. The distances between the *pro-R* hydrogen of the C4 of the dihydronicotinamide ring to C7 of PhCHO plotted vs the angle formed by C4 to *pro*-R hydrogen to C7 of PhCHO. NAC structures are in the lower right box and amount to 12% of conformers.

p-character at the C4−H_R bond allowing greater orbital overlap throughout the trajectory. The ring puckering conformation for NADH (in MD3) is now considered.

Figure 11 presents the conformational distribution of the ring-puckering angle α_C in MD3 (see Chart 4). The center of the population of α_C (Figure 11) is located at 4.0°. Forty-five percent (45%) of the sampling population of α_C is beyond 5.0° and the *pro*-R hydrogen is in the axial position, and 11% of the sampling population of α_C is beyond 10.0°. The center of the population of α_n (Chart 4) is located at 0.5°. The glycosidic torsional angle for the C−O bond, χ_n (Chart 4), converged to anti during the dynamics simulation. In the MD3 simulation, the torsion angle χ_n in the NADH conformation resides at an average of −120°. The equilibration took around 500 ps to converge to the anti −120°. Houk et al.[25] carried out ab initio calculations using

Table 3. Heavy Atom Distances at the Active Site for MD3

atoms		distances (Å)
NC4	C7	4.17
O1	48OG	2.57
48OG	NO2′	2.76
NO2′	51NE2	3.00
NO2′	NO3′	3.00
NO3′	51NE2	3.12
NO3′	269O	2.77
51ND1	WatAO	3.05
51NE2	WatAO	
269O	WatBO	2.73
Zn	O1	2.18

Chart 4

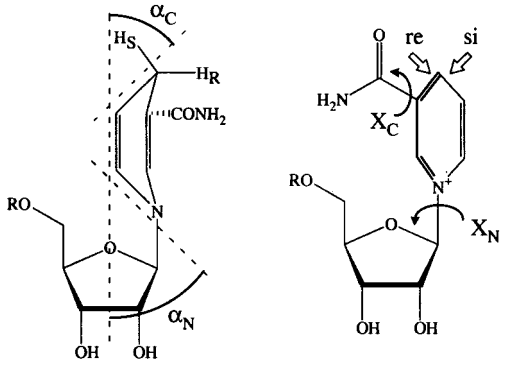

N-hydroxymethyl (in place of 1-ribosyl)-1,4-dihdropyridine to correlate the glycosidic torsional angle for the C−O bond with the puckering angles α_n and α_c. Their calculated C−O bond torsional angle χ_n, associated with the largest values of α_n and α_c, was 130°.

We have previously observed puckering[28] in ab initio transition structures for the general base-catalyzed C4 deprotonation of *N*-methyl-1,4-dihydronicotinamide radical cation to

(28) Olson, L. P.; Bruice, T. C. *Biochemistry* **1995**, *34*, 7335−7347.

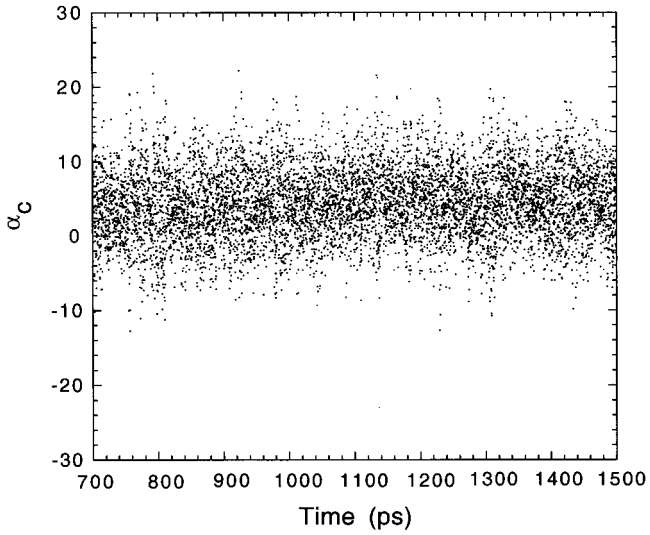

Figure 11. The histogram of the ring-puckering angles α_C of the NADH during the MD3 dynamics run. The center of the population of α_C is at 4°. 45% of the sampling population of α_C is beyond 5.0° and the *pro-R* hydrogen is in the axial position, and 11% of the sampling population of α_C is beyond 10.0°.

provide the neutral radical. Ring puckering appeared to provide a kinetic advantage, assisting in the departure of the H^+.[15,27] Aside from electronic effects, the anisotropic bending of the dihydronicotinamide toward the substrate is of kinetic importance in the positioning of reactants.

Kinetic isotope effects are among the few experimental observables that can provide information concerning transition state structures. Temperature and substituent effects upon k^H/k^D were found to be in accord with a significant contribution of tunneling to the rate of dihydronicotinamide reductions in enzymatic[29] and model[30] systems (see also res 31 and 32). By use of a combination of canonical variation transition state theory (adjusted AM1) for barrier dynamics and optimized multidimensional paths for tunneling, Alhambra et al.[7] find tunneling to account for 60% of the product in the HLADH·NAD^+·$PhCH_2O^-$ → HLADH·NADH·PhCHO reaction.

Conclusion

Nanosecond molecular dynamic simulations of the motions of the HLADH·$PhCH_2OH$·NAD^+ (MD1), HLADH·$PhCH_2O^-$·NAD^+ (MD2), and HLADH·PhCHO·NADH (MD3) systems have been carried out. The reduction of NAD^+ by $PhCH_2OH$ follows MD1 → MD2 + H^+ followed by MD2 → MD3. Hydride transfer is rate determining. In MD2 approximately 60 mol % of conformers are found in which the nicotinamide C4 and the *pro*-R hydrogen of $PhCH_2O^-$ are so arranged (NACs) that reactants can enter the transition state for hydride transfer from alkoxide to NAD^+. The alkoxide oxygen of $PhCH_2O^-$ is stabilized by association with the active site zinc. The mole percentage of NACs for the retro reaction is ∼12 mol % of conformers.

On MD1 → MD2 + H^+ the proton is transferred to water solvent via His51 through a relay consisting of two possibilities: (1) $PhCH_2OH$···Ser48-OH···Ribose 2′-OH···His51···H_2O and (2) $PhCH_2OH$···Ser48-OH···Ribose 2′-OH···Ribose 3′-OH···H_2O (Chart 1). For path **1**, the average hydrogen bonding distances between $PhCH_2OH$, Ser48-OH, ribose 2′-OH, and Hist51-Im are between 2.0 and 2.1 Å; and for path **2**, the average hydrogen bonding distances between $PhCH_2OH$, Ser48-OH, ribose 2′-OH, ribose 3′-OH, and Hist51-Im are between 2.0 and 2.1 Å. MD tracking of a molecule of water to the active site established that the water may accumulate at either of two sites such that transfer of H^+ away from the active site may be either to water from His51 (from Nϵ2 or Nδ1) and from NAD^+ ribose 3′OH.

Acknowledgment. This work was supported by a grant from the National Institutes of Health (5R37DK09171-36). The computation was supported in part by NSF cooperative agreement ACI-9619020 through computing resources provided by the National Partnership for Advanced Computational Infrastructure at the San Diego Supercomputer Center.

JA0109747

(29) Klinman, J. P. *Biochemistry* **1976**, *15*, 2018−2026. Klinman, J. P. *CRC Crit. Rev. Biochem.* **1981**, *10*, 39−78.

(30) Powell, M. F.; Bruice, T. C. *J. Am. Chem. Soc.* **1983**, *105*, 7139−7149.

(31) Cha, Y.; Murray, C. J.; Klinman, J. P. *Science* **1989**, *243*, 1325−1330. Cha, Y.; Murray, C. J.; Klinman, J. P. *Science* **1989**, *243*, 1325−1330.

(32) Sinha, A.; Bruice, T. C. *J. Am. Chem. Soc.* **1984**, *106*, 7291−7292.